Spectrochimica Acta Part A: Molecular and Biomolecular Spectroscopy 233 (2020) 118197

Contents lists available at ScienceDirect

Spectrochimica Acta Part A: Molecular and Biomolecular Spectroscopy

journal homepage: www.elsevier.com/locate/saa

Design a fluorometric aptasensor based on CoOOH nanosheets and carbon dots for simultaneous detection of lysozyme and adenosine triphosphate

Zeinab Saberi [a], Behzad Rezaei [a,*], Parisa Rezaei [b], Ali Asghar Ensafi [a]

[a] Department of Chemistry, Isfahan University of Technology, Isfahan 84156-83111, Islamic Republic of Iran
[b] Department of Medical Laboratory Science, School of Medicine, Isfahan University of Medical Sciences, Isfahan, Iran

ARTICLE INFO

Article history:
Received 24 December 2019
Received in revised form 20 February 2020
Accepted 23 February 2020
Available online 29 February 2020

Keywords:
Simultaneous detection
Aptasensor
Carbon dots
Nanosheets
Lysozyme
Adenosine triphosphate

ABSTRACT

Simultaneous detection of biomarkers and biomolecules with great analytical performance still is challenging. A simple fluorometric dual-functional aptasensor was designed to detect Lysozyme (LYS) and adenosine triphosphate (ATP) as models of a protein and a small molecule simultaneously. The sensing principle of the aptasensor is based on the interactions between cobalt oxyhydroxide CoOOH nanosheets as fluorescence quencher and carbon dots (CDs) as fluorophores. The aptamer labeled with CDs was able to assemble on CoOOH nanosheets and consequently, the fluorescence signal was quenched. With addition target analytes to the system, the aptamers folded around of targets with a strong and specific affinity. Therefore, the labeled aptamer with CDs was detached from CoOOH nanosheets and the fluorescence signal was restored. The fluorescence spectral overlap of these two CDs is the main limitation for the simultaneous analysis. The least squared support vector machine (LS-SVM) was applied to resolve this problem. Under optimal conditions, when LS-SVR was used, detection limits were found 4.0 and 1.8 nmol L^{-1} for ATP and LYS. The parallel biosensor is capable of monitoring ATP and LYS levels in the biological samples with satisfactory results.

1. Introduction

The use of biomarkers has become common in basic and clinical researches. The presence and level of biomarkers such as nucleic acids, proteins, and carbohydrates are a signal of a specific disease, especially cancer. So, the development of a selective and sensitive assay for detecting these biomarkers is a critical goal in the biosensing [1,2]. Until now, the simultaneous measurement of biomarkers or molecules has remained a challenge between scientists [3].

LYS or muramidase is known as a ubiquitous antimicrobial enzyme with a single polypeptide chain and a molecular weight of 14 kDa [4]. Among several protein biomarkers, LYS plays an important role in the various organisms and prevents several bacterial infections. It has been used as a model for enzyme catalysis and applied in proteomics. Also, other uses of LYS are in the wine industry, cheese production, and medicine such as an anti-inflammatory drug. The level of LYS is a key biomarker for identifying several diseases such as sarcoidosis, monocytic or myelomonocytic leukemia and bronchopulmonary dysplasia [5].

ATP, well-known as energy unit currency, was found in the cytoplasm and nucleoplasm of all living cells. It plays a fundamental role in most enzymatic activities. The concentration of ATP is an indicator of cell viability and many diseases such as Parkinson's disease, malignant tumors and Alzheimer's disease [6].

Simultaneous sensing of ATP and LYS is considered by scientists in the clinical diagnosis and biomedicine studies that it remains a challenge. Some aptasensors have been reported for parallel detection of LYS and ATP and their analogues, including Resonance light scattering (RLS) [7], surface-enhanced Raman scattering (SERS) [8], and electrochemistry [9]. These methods have several disadvantages such as expensive, needed amplification steps and skilled personnel. To overcome these drawbacks, the fluorescence aptasensors have been drawn more attention due to high sensitivity, good selectivity, and simplicity without complicated pretreatment [10]. However, only a few optical and electrochemical aptasensors have been designed for the analysis of various analytes simultaneously [11–13].

Nucleic acid aptamers are single-stranded DNA that binds to their targets tightly and selectively through van der Waals forces, hydrogen bonding, and electrostatic interactions [14]. In comparison with antibodies, aptamers have low-toxicity and little immunogenicity [15]. Also, aptamers are smaller than antibody molecules that can penetrate into the tumor tissues. So, the aptamer-based biosensors have been used for detecting a vast range of metal ions and small molecules (e.g. ATP, adenosine) or too large proteins (e.g. lysozyme, thrombin) and especially biomarkers in clinical treatment and cancer diagnosis [16,17].

* Corresponding author.
E-mail address: rezaei@cc.iut.ac.ir (B. Rezaei).

https://doi.org/10.1016/j.saa.2020.118197
1386-1425/

Carbon dots (CDs) have emerged as a member of the photoluminescent nanomaterials characterized by a size lower than 10 nm. In comparison with common fluorescent labels such as organic dyes and semiconductor quantum dots, CDs possess intriguing properties such as high aqueous solubility, low cytotoxicity, biocompatibility and high resistance to photobleaching. With these characterizations, CDs have been regarded in the biomedical, optoelectronic, and photocatalytic applications [18]. Various techniques have been reported for the synthesis of CDs including laser ablation [19], microwave [20], and hydrothermal treatment [21]. The use of the hydrothermal method provides benefits such as facile synthesis, high efficiency and inexpensive. CDs could be synthesized from various carbon-based chemical compounds and raw materials.

Over the past decade, two-dimensional (2D) nanomaterials such as transition metal dichalcogenides (TMDCs) and transition metal oxyhydroxide nanosheets have received more attention because of their unique electronic, optical and catalytic properties, possessing the fluorescence quenching activity and biocompatibility. Due to a large surface area and planar structure, biomolecules such as proteins or nucleic acids were able to absorb on the nanosheets through noncovalent interactions that make them great potential in the biosensing applications [22]. CoOOH nanosheets are a type of 2D nanostructure that recently, they have been applied as the quenchers of fluorescence emission due to specific properties including large surface areas, good charge transfer rate, and optical absorbance [23–25].

In the spectroscopic parallel study, spectral bands overlapping often occur severely that it is difficult to distinguish the response of species due to their overlapping. The use of chemometric methods can be overcome on the overlapping problem and identify the species involved in the system. Various applications of the multivariate methods have been reported by researchers to resolve the spectra overlapping for quantitative determination in the spectroscopy. In this study, the LS-SVM method was used for the treatment of overlapping [26]. LS-SVM is a modified version of SVM proposed by Suykens et al. [27] that it was applied for quantification and classification [28,29]. So, the LS-SVM algorithm is described briefly. LS-SVM fits a linear relation ($y = wx + b$), between the regressors (x) and the dependent variables (y) that **w** and **b** are the weight vector and the model offset, respectively. The best relation was obtained when the cost function (Q) was minimized that containing **w** and regression errors in the training set:

$$Q = \frac{1}{2} w w^T + \frac{1}{2}\gamma \sum_{i=1}^{N} e_i^2 \quad (1)$$

subject to

$$y_i = w^T \varphi(x_i) + b + e_i \; i = 1 \ldots N \quad (2)$$

that Q indicates the feature map. The first part of the Q function is used to regularize weight sizes and penalize large weights and the second part minimizes the error of training data. The relative weight of this part as compared to the first part was denoted by the parameter γ, which must be optimized. The performance of LS-SVM depends on the combination of several parameters. SVM regression is based on kernel substitution that the most used kernel type is the radial basis function (RBF), exp. $(-(\|xi\text{-}xj\|^2)/2\sigma^2)$, a simple Gaussian and polynomial functions where σ^2 is the width of the Gaussian function. It is necessary to do careful tuning of the RBF kernel constant and γ regularization constant, to achieve a good generalization model.

Herein, LYS and ATP were simultaneously detected using parallel fluorometric aptasensor. There is no report about the simultaneous fluorescence sensing of ATP and LYS. For this aim, CoOOH nanosheets and labeled aptamers with different CDs were applied as a quencher and probes respectively.

2. Experimental

2.1. Chemicals and apparatuses

The 5′-amino-modified anti Lysozyme aptamer (5′-ATCAGGGCTAA AGAGTGCAGAGTTACTTAG-3′) [30] and the 5′-amino-modified DNA oligonucleotides (5′-TTTTTTACCTGGGGGAGTATTGCGGAGGAAGG-3′) [6] for ATP aptamer were prepared in Oligo Macrogen (Seoul, South Korea). The materials including ATP, Lysozyme, KCl, Na_2HPO_4, N-hydroxy sulfosuccinimide sodium salt (NHS), KH_2PO_4 and 1-ethyl-3-(3-dimethyl aminopropyl) carbodiimide hydrochloride (EDC), were obtained from Sigma-Aldrich. $CoCl_2 \cdot 6H_2O$ and NaClO were provided by Riedel-DeHaan (Seelzet, Germany).

Fluorescence spectra were measured on a spectrofluorimeter model Jasco FP-750 (Tokyo, Japan) with excitation and emission slit widths set at 5.0 nm. Transmission electron micrograph (TEM) analysis was obtained with Philips, Model CM30 using an accelerator voltage of 300 kV. a Jasco V–570 UV/Vis/NIR spectrophotometer (Tokyo, Japan) was used for measuring UV–visible absorbance spectra by a 1 cm path length cell. Fourier-transform infrared spectra were taken on an FTIR model 350 (Jasco Co., Tokyo, Japan). X-ray Diffraction (XRD) method was applied for investigating the crystal structure of the CDs and CoOOH nanosheets using a Bruker D8 advance X-ray Diffractometer. Morphology of nanosheets was investigated using a field emission scanning electron microscope (FE-SEM, HITACHI S-4160).

2.2. Preparation of two CDs

The hydrothermal method was employed for the synthesis of two kinds of CDs. CDs1 and CDs2 were prepared from citric acid-ethylene diamine [31] and orange juice [32], respectively. More details of preparations are presented in the “supplementary materials”.

2.3. Conjugation of CDs with aptamer

To conjugate the aptamers and CDs covalently, the standard EDC procedure was utilized [33]. In brief, 32 μL EDC/NHS solution and the CDs diluted with phosphate buffer were mixed for functionalizing the surface carboxylic groups of CDs and shaken at room temperature for 1 h. Then, 20 μL of the aptamer (100 μM) was added to the mixture and it was allowed to react for 6 h at room temperature with continuous shaking. Finally, the resulting solution was filtered with Sartorius 10 kDa molecular weight cutoff spin filter to eliminate the excess reagents at 3000 rpm for 20 min. The product was stored at 4 °C and dark place. CDs1 and CDs2 have conjugated to LYS and ATP aptamer, respectively.

2.4. Synthesis of the CoOOH nanosheets

The CoOOH nanosheets have been prepared according to the previous procedure [34]. Firstly, a solution was prepared by mixing NaOH (1.0 M, 125 μL) and $CoCl_2.6H_2O$ (10.0 mM, 500 μL) in a tube under ultrasound for 1 min. Then, NaClO (0.9 M, 25 μL) was added to the solution and sonicated again for 10 min. Subsequently, the centrifuged precipitate was purified with deionized water at least three times. Ultimately, the nanosheets were collected and kept at 4 °C.

2.5. Preparation of real samples

Human blood plasma and urine samples were got from the Health Center of Isfahan University of technology. The blood plasma and urine samples were filtered and diluted 20 and 40 times by the phosphate buffer (pH = 7.4), respectively. Various concentrations of ATP and LYS were spiked in the biological samples.

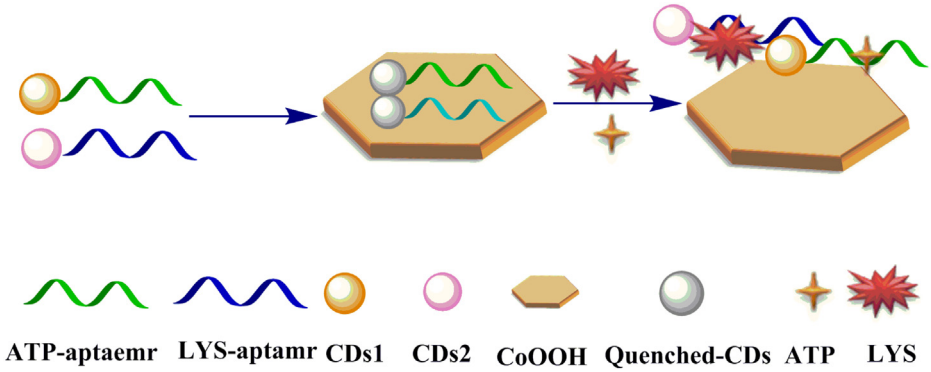

Scheme 1. Schematic illustration of a parallel aptasensor for fluorescent analysis of ATP and LYS.

3. Results and discussions

3.1. The principle detection of aptasensor

Scheme 1 illustrates the principle of developed aptasensor for the simultaneous detection of ATP and LYs. The mixing probe solution contains CDs1 and CDs2 were excited at the same wavelength of 340 nm. With additional certain amount of CoOOH nanosheets to the solution, the CDs2-ATP aptamers and CDs1-LYS aptamer could be adsorbed on the nanosheets surface through the van der Waals forces among nucleobases of aptamer and the basal plane of nanosheets. The fluorescence signal of mixing probes was quenched. Upon the addition

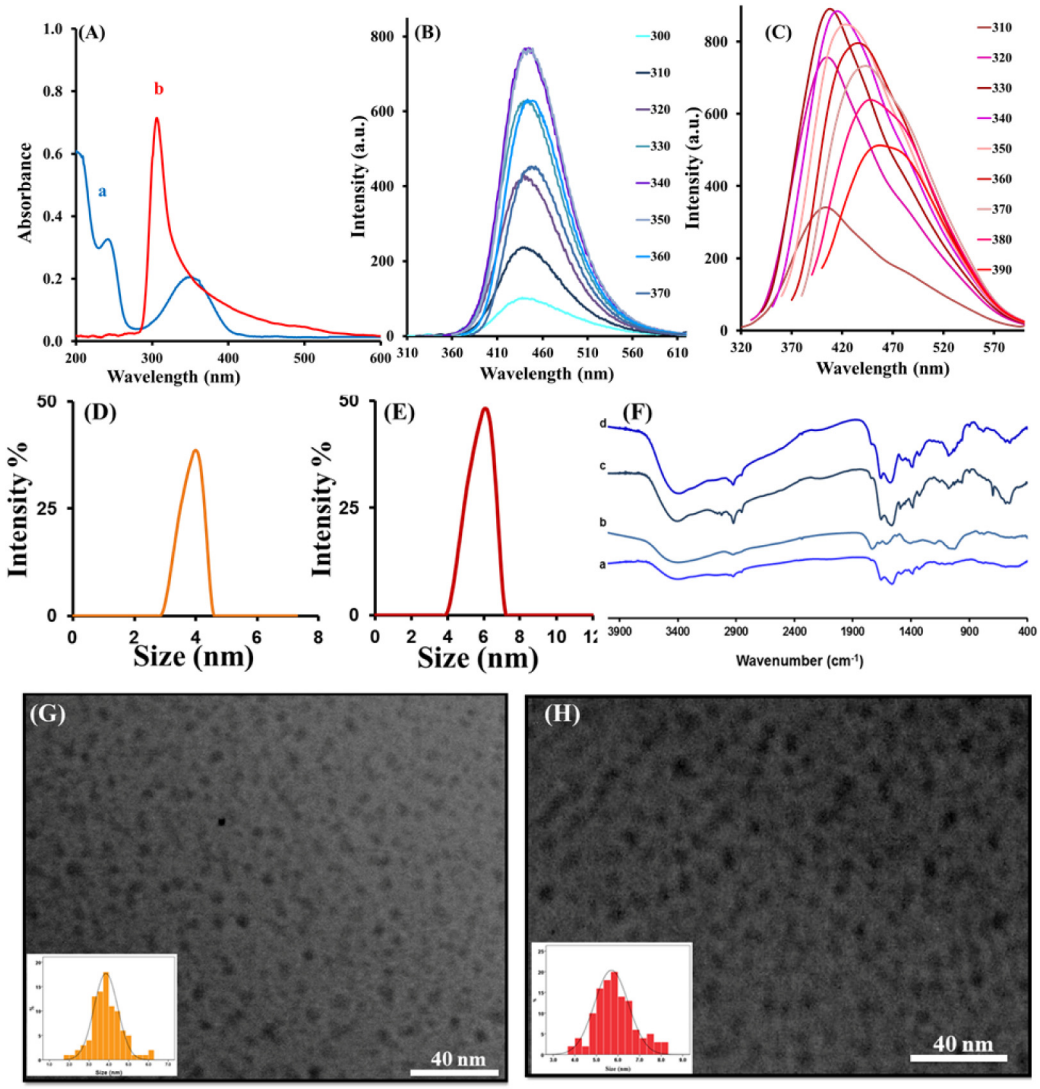

Fig. 1. (A) UV–Vis spectrum of CDs1 (curve a) and CDs2 (curve b); (B) Fluorescence spectra of CDs1 at different excitation wavelengths; (C) Fluorescence spectra of CDs2 at different excitation wavelengths; (D) DLS diagram of CDs1; (E) DLS diagram of CDs2; (F) FT-IR spectra of (a) CDs1; (b) CDs2; (c) CDs1 conjugated to LYS-aptamer; (d) CDs2 conjugated to ATP-aptamer. (G) TEM image of CDs1 and (H) CDs2;

of ATP and LYS, aptamers wrapped around their targets with a strong affinity and released from CoOOH nanosheets. As a result, the quenched fluorescence signal would restore and be proportional to the amounts of ATP and LYS. The possible mechanism of fluorescence quenching can be related to Förster resonant energy transfer (FRET) based on overlapping the UV–Vis spectrum of CoOOH nanosheets and fluorescence spectra of CDs.

3.2. Characterization of CDs1 and CDs2

CDs can be synthesized from organic compounds or raw carbonaceous materials. CDs have advantages included high solubility, high quantum yield and the presence of carboxylic groups on their surface which able to conjugated covalently to the biomaterial. On the basis of these reasons, CDs were chosen for this study. The formation of CDs is based on the carbonization of citric acid and constituents in orange juice.

Simultaneous detection of ATP and LYS was done by exciting CDs1-LYS-aptamer and CDs2-ATP-aptamer at the same excitation wavelength. The UV–Vis absorbance spectra of CDs1 and CDs2 are shown in Fig. 1 A. Clearly, their wide absorbance peaks indicate that they can be by a single wavelength. CDs1 spectrum (curve a) shows absorbance bands at 242 and 344 nm, related to the π-π* transitions of C═C and n-π* transitions of C═O, respectively. The absorbance peak at 303 nm of CDs2 spectrum (curve b) is due to the π-π* transitions [32]. Fluorescence emission is one of the most special attractions of CDs that their excitation wavelength dependence is a common behavior in the CDs that may arise from different sizes of particles and distribution of emissive domains. The fluorescence properties of CDs1and CDs2 are illustrated in Fig. 1 B, C. The fluorescence peaks of CDs1 and CDs2 shift from 438 to 446 nm and 404 to 458 nm when excitation wavelengths change from 310 to 380 nm, respectively. The existence of functional groups on the CDs surface with different state energy levels can be the reason for the excitation wavelength-dependent behavior of CDs. DLS method was utilized to gain an average diameter and distribution of CDs1 and CDs2 particles. DLS diagrams of CDs1 and CDs2 in Fig. 1D and E show the average size of CDs1 and CDs2 that are around 3.7 and 5.8 nm, respectively. The functional groups of both CDs were investigated by FT-IR spectroscopy. FT-IR spectra (Fig. 1Fa,b) show many oxygenated functional groups on their surfaces such as O—H broad peak at 3300 cm^{-1}, around 1160 and 1130 cm^{-1} can be attributes to C—O—C bonds and C—O bonds at 1360 and 1310 cm^{-1}. The absorbance peaks at 1730 and 1640 cm^{-1} confirm the C═O bonds, whereas the peaks at 2907 and 2845 are assigned to C—H bonds. The way to monitor the conjugation CDs to aptamer is FT-IR spectroscopy (Fig. 1Fc, d). Vibrational peaks at 963, 1014 cm^{-1} can be related to C—C/C—O deoxyribose skeletal motions and P—O/C—O stretching, respectively. Moreover, the absorbance peaks at 835 and 780 cm^{-1} are indicative of the deoxyribose phosphate and sugar-phosphate vibration modes [6]. The morphology and size of CDs were indicated by TEM method (Fig. 1G, H). Images show the round shape of CDs and also, average sizes of CDs1 and CDs2 are obtained 3.8 and 5.8 nm using statistical analysis that confirms the DLS results. The XRD pattern of both CDs shows a broad peak at around $2\theta = 20$ that is be related to the (002) diffraction planes of amorphous carbon materials (Fig. S1).

3.3. Characterization of CoOOH

CoOOH nanosheets were synthesized with good stability through oxidizing and exfoliating cobalt hydroxide nanosheets. The structural and morphological information of nanosheets were studied using SEM, FT-IR, XRD and EDX methods. Fig. 2A illustrates the FT-IR spectrum of CoOOH nanosheets. The peaks at around 600 and 1600 cm^{-1} are indicative of Co-O^{-2} complex in the oxide and Co—O bond, respectively. The broad peak at 3420 cm^{-1} revealed the O—H stretching vibrations [35]. The surface morphology studies indicate a hexagonal structure of CoOOH nanosheets with a thickness of less than 5 nm and sidelong dimensions of about 50 nm in Fig. 2B. In the XRD pattern (Fig. S2A), CoOOH nanosheets show several diffraction peaks at around $2\Theta = 20$, 38, 52 that are indexed to (003), (012) and (018) planes, which confirm the hexagonal structure. EDX analysis was applied for confirming the composition of CoOOH nanosheets with the presence of peaks related to elements Co and O in Fig. S2B. [34].

3.4. Optimization of the assay conditions

To achieve the best analytical performance, several parameters including CoOOH sheets concentration, incubation and recovery time were optimized. The UV–visible absorbance spectrum of the CoOOH nanosheets was overlapped with fluorescence spectra of the CDs1 and CDs2 (Fig. S3). It shows that the mechanism of fluorescence quenching can be energy transfer. With the addition CoOOH nanosheets to the system, fluorescence signals were reduced. So, the nanosheets concentration was optimized for the maximum quenching efficiency. As shown in Fig. S4 A, B, and C, fluorescence signals of CDs1-LYS-aptamer and CDs2-ATP-aptamer were been reduced when CoOOH concentrations were increased. Thus, 0.22 mg/mL was chosen as an optimized concentration for the mixing probes. Adsorption of CDs-aptamer on the CoOOH surface and recovery of fluorescence signals are time-dependent. So, upon the addition of optimal CoOOH concentration, the fluorescence signals were monitored. As shown in Fig. S5, the fluorescence emission decreased and reached a plateau after 25 and 30 min for individual and mixing detection. Also, it is illustrated in Fig. S6, the fluorescence of CDs was increased within 35–50 min and next remained constant. In the following experiments, 30 and 50 min were taken as incubation and

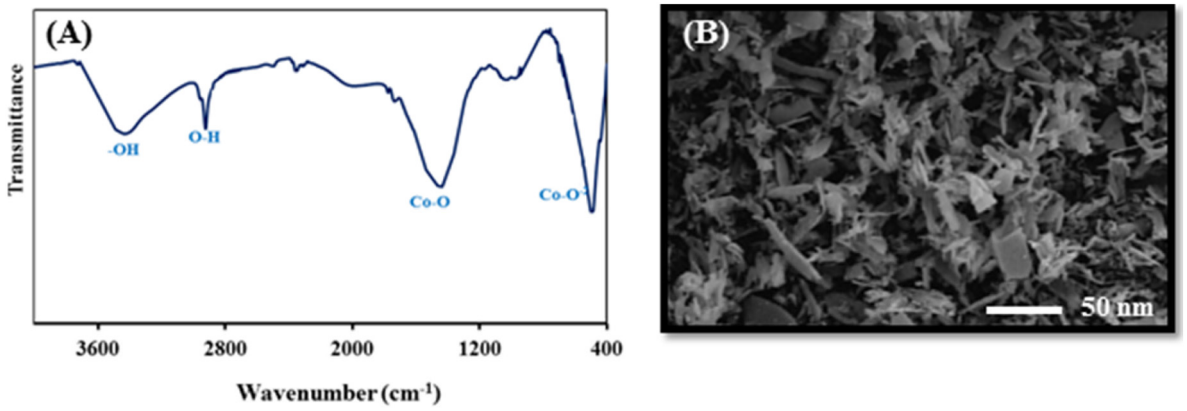

Fig. 2. (A) FT-IR spectrum; (B) FE-SEM image of CoOOH nanosheets.

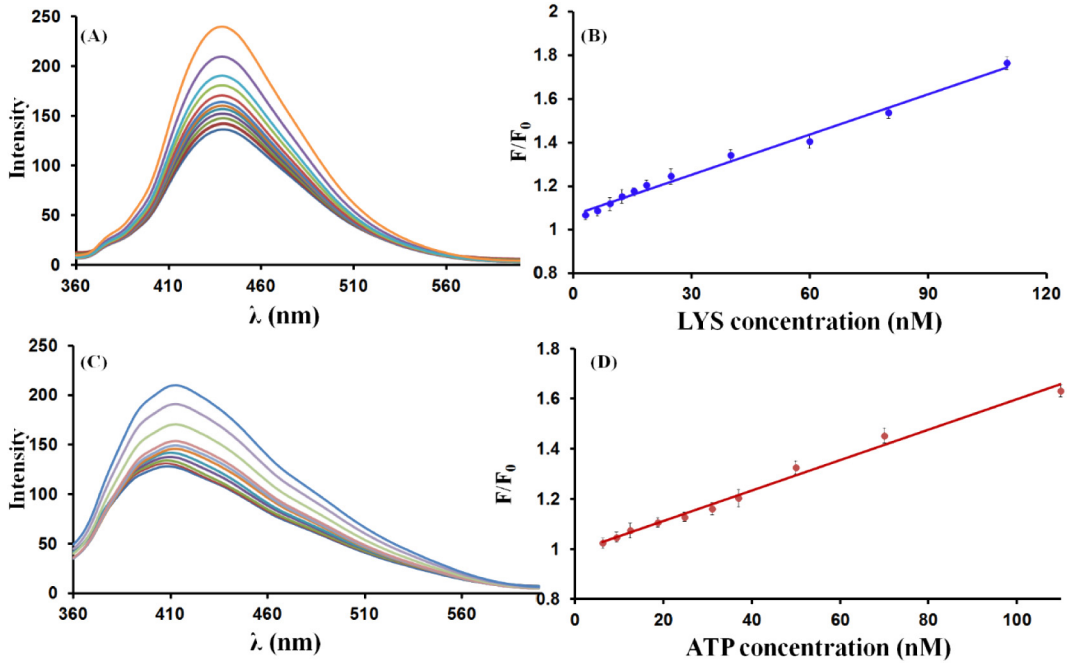

Fig. 3. (A) The fluorescence spectra of CoOOH-CDs1-LYS-aptamer under different concentration (0-110 nM). (B) calibration curve of ATP aptasensor. (C) The fluorescence spectra of CoOOH-CDs2-ATP-aptamer in presence of different concentration (0–105 nM). (D) calibration curve of LYS aptasensor.

recovery times for the mixing probe, respectively. All experiments were performed at room temperature and at physiological pH (pH = 7.4).

3.5. Performance of aptasensor

The designed aptasensor can be used for the detection of ATP and LYS individually and simultaneously. To investigate these applications, the fluorescence emissions were monitored after the addition of ATP or LYS at several concentrations under optimized conditions, separately. Fig. 3A, B shows the fluorescence changes of LYS-aptamer conjugated to CDs1 versus increasing the LYS concentration. The linear range for LYS was obtained 3.1–110 nmol L^{-1} ($R^2 = 0.9906$) with 0.3 nmol L^{-1} as the detection limit based on the 3 s/m which "s" was the standard deviation for 10 blank samples and "m" was the slope of the calibration line. As shown in Fig. 3C, D, the fluorescence intensity of ATP-aptamer labeled with CDs2 increased after the addition of ATP to the system with a good linear relation ($R^2 = 0.9891$) in the range from 6.2 to 110 nmol L^{-1}. The limit of detection was found at 4.0 nmol L^{-1}. In order to the simultaneous determination in the mixture, the chemometric methods were used to treat the fluorometric spectra. On the other hand, the LS-SVM algorithm was applied to overcome the overlapping of spectra in Fig. S7A. The LYS and ATP concentrations were varied between 3.1–90 and 6.2–105 nmol L^{-1}, respectively. To evaluate the calibration model, coefficients of determination (R^2) of plots of measured versus predicted values, the root means a square error of calibration (RMSEC) and relative standard error of prediction (RSEP) can be applied that [36]:

$$RMSEC = \sqrt{\frac{\sum_{i=1}^{n}(C_{pred} - C_{obs})^2}{n}} \quad RSEP\% = 100 \times \sqrt{\frac{\sum_{i=1}^{n}(C_{pred} - C_{obs})^2}{\sum C_{obs}{}^2}}$$

where C_{obs} and C_{pred} are the observed and the predicted value of concentration in the sample and n is the number of samples in the prediction set.

The ideal model has high R^2 value with low RMSEC and RSEP values. The R^2 of the calibration curves for ATP and LYS has been found 0.9990 and 0.9978 in Fig. S7 B, C, respectively, that indicates the good calibration. Some obtained results from the simultaneous determination of LYS and ATP with levels of RSEP and RMSEC and the percentage error are shown in Table 1. As can see, acceptable quantitative results were provided by the LS-SVM algorithm. Based on the results of the model, the detection limit of 1.8 and 4.0 nmol L^{-1} was found for ATP and LYS, respectively. The optimized values of (γ, σ^2) were obtained (9422,10.35) and (7128, 12.23) for ATP and LYS, respectively.

Whereas complex matrix samples can contain possible interferences that have an influence on the sensing system, it is essential to evaluate the selectivity of a biosensor for clinical applications. The selectivity of the aptasensor to LYS and ATP toward some homologous compounds (including guanosine triphosphate (GTP), cytidine triphosphate (CTP), and Uridine triphosphate (UTP) as controls for detection of ATP and Bovine serum albumin (BSA), Human serum albumin (HSA), and Bovine Hemoglobin (BHb) as controls for detection of LYS) was investigated at concentration 50 nmolL^{-1} for LYS and ATP and 500 nmolL^{-1} for homologous compounds at same optimized conditions. As shown in Fig. 4 and Fig. S8, the significant fluorescence enhancement was observed in the presence of ATP and LYS, while the influence of other components was not notable responses. The results demonstrate that the proposed

Table 1
Prediction results and quality parameters of SVM calibration model for simultaneous determination of ATP and LYS.

Concentration (nmol L^{-1})		Predicted concentration (nmol L^{-1})		Relative error %	
ATP	LYS	ATP	LYS	ATP	LYS
10.2	90	10.34	87.6	−1.3	2.6
22.4	15.5	22.24	16.4	0.7	−5.4
30.0	30.0	30.2	28.7	−0.7	4.3
90.7	8.1	90.4	7.6	0.3	6.1
RMSEC[a]		0.12	0.091		
RSEP (%)[b]		5.0	4.1		
R^2		0.99	0.99		
σ^2		10.35	10.23		
Γ		9422	7128		

[a] Root mean square error of calibration.
[b] Relative standard error of prediction.

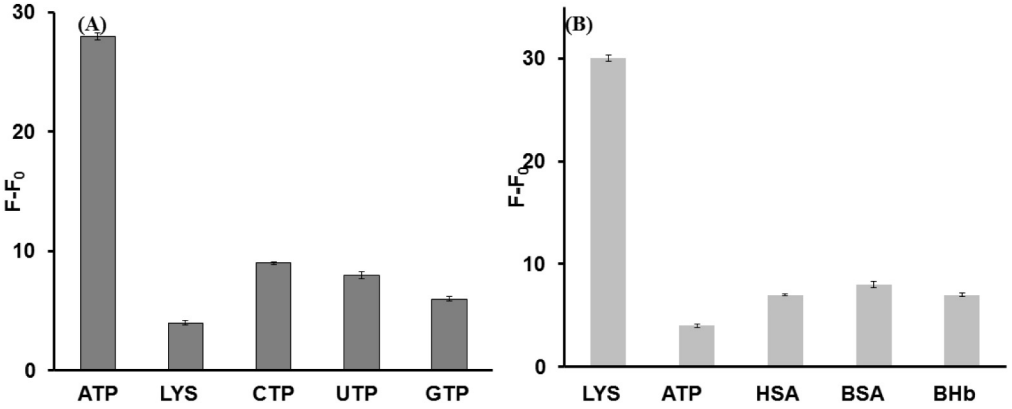

Fig. 4. The selectivity of CDs1-LYS aptasensor and CDs2-ATP aptasensor for detection LYS and ATP toward their analogues compounds.

biosensor based on CDs fluorescence can recognize ATP and LYS molecules with high selectivity and make a potential for practical detection.

Table 2 shows the comparison of results of this work with previously reported researches for the simultaneous detection of ATP and LYS. The analytical performance of methods indicates that the proposed assay is comparable to others with good sensitivity and selectivity. So, the introduced sensor can be as a novel and successful parallel aptasensor for ATP and LYS detection.

3.6. Detection ATP and LYS in the real sample

In order to investigate the potential of the proposed aptasensor in the complicated biological samples, the procedure was applied to the simultaneous determination of the ATP and LYS content in the diluted healthy human serum and urine samples. For this propose, 20 μL of diluted biological samples was added to quenched CDs-aptamers mixture under optimized conditions. As a result, no significant recovered fluorescence was observed after addition. So, various concentrations of ATP and LYS were spiked to the human serum and added to the solution. The obtained results were reported in Table S1 indicating that designed biosensor can be an effective tool for detecting analytes in the biological environment.

4. Conclusion

In summary, an effective fluorescence aptamer sensing method based on CDs and CoOOH nanosheets has been designed to detect ATP and LYS simultaneously for the first time. Since the fluorescence spectra of CDs1 and CDs2 conjugated to aptamers are overlapped, the chemometric tools were used to deconvolute the overlapped spectra. This parallel assay based on aptamers presents several advantages such as selectivity, sensitivity, and ease for simultaneous detection of small molecules and protein as targets. It is worth to mention that unlike SERS and RLS methods that need the complex instruments and high-skilled staff, the proposed method has simplicity, cost-efficient, and fast analysis. Also, this method could be used as a great tool in biological applications.

CRediT authorship contribution statement

Zeinab Saberi: Conceptualization, Methodology, Software, Writing - original draft. **Behzad Rezaei:** Supervision, Writing - original draft, Writing - review & editing. **Parisa Rezaei:** Visualization, Investigation. **Ali Ashghar Ensafi:** Supervision.

Acknowledgments

We wish to thank the Center of Excellence in Sensor and Green Chemistry and Research Council of Isfahan University of Technology (IUT) and Iran National Science Foundation (INSF) for their patronage and help in this study.

Declaration of competing interest

The authors declare that they have no known competing financial interests or personal relationships that could have appeared to influence the work reported in this paper.

Appendix A. Supplementary data

Supplementary data to this article can be found online at https://doi.org/10.1016/j.saa.2020.118197.

References

[1] J.F. Rusling, C.V. Kumar, J.S. Gutkind, V. Patel, Measurement of biomarker proteins for point-of-care early detection and monitoring of cancer, Analyst 135 (2010) 2496–2511.
[2] L. Wu, X. Qu, Cancer biomarker detection: recent achievements and challenges, Chem. Soc. Rev. 44 (2015) 2963–2997.
[3] Z.S. Qian, X.Y. Shan, L.J. Chai, J.R. Chen, H. Feng, Dual-colored graphene quantum dots-labeled nanoprobes/graphene oxide: functional carbon materials for respective

Table 2
Comparison of designed aptasensor and other reported aptasensors for the simultaneous determination of ATP and LYS.

Technique	LOD_{ATP} (nmol L^{-1})	LOD_{LYS} (nmol L^{-1})	Linear range (nmol L^{-1})	Reference
Resonance light scattering (RLS)	0.01	0.001	LYS: 5.0–100 ATP: 2.5–75.0	[7]
Surface-enhanced Raman scattering (SERS)	0.01	10^{-5}	LYS: 10^{-5}-0.01 ATP: 0.05–10.0	[8]
Electrochemical method	4.8	0.12	LYS: 0.2–10.0 ATP: 10.0–10^4	[9]
Fluorometric assay	1.8	4.0	LYS: 3.1–90 ATP: 4.2–105	This work

and simultaneous detection of DNA and thrombin, Nanotechnology 25 (2014) 415501.
[4] Y.N. Khonsari, S. Sun, A novel label free electrochemiluminescent aptasensor for the detection of lysozyme, Mater. Sci. Eng. C. 96 (2019) 146–152.
[5] S. Pawar, K. Raul, D. Ottoor, Investigation of complexation of amlodipine with lysozyme and its effect on lysozyme crystal growth, Spectrochim Acta Part A 227 (2020), 117623.
[6] Z. Saberi, B. Rezaei, T. Khayamian, A fluorescent aptasensor for analysis of adenosine triphosphate based on aptamer–magnetic nanoparticles and its single-stranded complementary DNA labeled carbon dots, Luminescence 33 (2018) 640–646.
[7] F. Chen, C. Cai, X. Chen, C. Chen, "Click on the bidirectional switch": the aptasensor for simultaneous detection of lysozyme and ATP with high sensitivity and high selectivity, Sci. Rep. 6 (2016) 18814.
[8] S. Ye, J. Xiao, Y. Guo, S. Zhang, Aptamer-based SERS assay of ATP and lysozyme by using primer self-generation, Chem Eur J 19 (2013) 8111–8116.
[9] X. Qian, Y. Xiang, H. Zhang, Y. Chen, Y. Chai, R. Yuan, Aptamer/nanoparticle-based sensitive, multiplexed electronic coding of proteins and small biomolecules through a backfilling strategy, Chem Eur J 16 (2010) 14261–14265.
[10] K. Ma, F. Zhang, N. Sayyadi, W. Chen, A.G. Anwer, A. Care, B. Xu, W. Tian, E.M. Goldys, G. Liu, "Turn-on" fluorescent aptasensor based on AIEgen labeling for the localization of IFN-γ in live cells, ACS sensors 3 (2018) 320–326.
[11] X. Zuo, H. Zhang, Q. Zhu, W. Wang, J. Feng, X. Chen, A dual-color fluorescent biosensing platform based on WS2 nanosheet for detection of Hg^{2+} and Ag^{+}, Biosens. Bioelectron. 85 (2016) 464–470.
[12] N. Duan, S. Wu, S. Dai, T. Miao, J. Chen, Z. Wang, Simultaneous detection of pathogenic bacteria using an aptamer based biosensor and dual fluorescence resonance energy transfer from quantum dots to carbon nanoparticles, Microchim. Acta 182 (2015) 917–923.
[13] J. Zhao, X. He, B. Bo, X. Liu, Y. Yin, G. Li, A "signal-on" electrochemical aptasensor for simultaneous detection of two tumor markers, Biosens. Bioelectron. 34 (2012) 249–252.
[14] S. Song, L. Wang, J. Li, C. Fan, J. Zhao, Aptamer-based biosensors, TrAC Trends Anal. Chem. 27 (2008) 108–117.
[15] C. Chen, S. Zhou, Y. Cai, F. Tang, Nucleic acid aptamer application in diagnosis and therapy of colorectal cancer based on cell-SELEX technology, NPJ precision oncology 1 (2017) 37.
[16] T. Lakshmipriya, S.C. Gopinath, Aptamer: A Versatile Probe in Medical Diagnosis, INNOSC Theranostics and Pharmacological Sciences 1 (2018) 14–19.
[17] R.K. Meena, D. Kamboj, K. Kumar, S. Karanwal, A brief review on Aptamer based biosensors for detection of environmental pollution, Int. J. Curr. Microbiol. App. Sci. 7 (2018) 1483–1489.
[18] F. Arcudi, L. Đorđević, M. Prato, Synthesis, separation, and characterization of small and highly fluorescent nitrogen-doped carbon NanoDots, Angew. Chem. 55 (2016) 2107–2112.
[19] H.P. Castro, V.S. Souza, J.D. Scholten, J.H. Dias, J.A. Fernandes, F.S. Rodembusch, R. dos Reis, J. Dupont, S.R. Teixeira, R.R. Correia, Synthesis and characterisation of fluorescent carbon nanodots produced in ionic liquids by laser ablation, Chem Eur J 22 (2016) 138–143.
[20] K. Jiang, Y. Wang, X. Gao, C. Cai, H. Lin, Facile, quick, and gram-scale synthesis of Ultralong-lifetime room-temperature-phosphorescent carbon dots by microwave irradiation, Angew. Chem. 57 (2018) 6216–6220.
[21] Z. Saberi, B. Rezaei, A.A. Ensafi, Fluorometric label-free aptasensor for detection of the pesticide acetamiprid by using cationic carbon dots prepared with cetrimonium bromide, Microchim. Acta 186 (5) (2019) 273.
[22] Y. Cen, Y. Yang, R.Q. Yu, T.T. Chen, X. Chu, A cobalt oxyhydroxide nanoflake-based nanoprobe for the sensitive fluorescence detection of T4 polynucleotide kinase activity and inhibition, Nanoscale 8 (2016) 8202–8209.
[23] S.G. Liu, D. Luo, L. Han, N.B. Li, H.Q. Luo, A hybrid material composed of guanine-rich single stranded DNA and cobalt (III) oxyhydroxide (CoOOH) nanosheets as a fluorescent probe for ascorbic acid via formation of a complex between G-quadruplex and thioflavin T, Microchim. Acta 186 (2019) 156.
[24] Y. Yang, Y. Cen, W.J. Deng, R.Q. Yu, T.T. Chen, X. Chu, An aptasensor based on cobalt oxyhydroxide nanosheets for the detection of thrombin, Anal. Methods 8 (2016) 7199–7203.
[25] H. Yan, Y. Liu, W. Ren, J. Shangguan, X. Yang, Cobalt oxyhydroxide modified with poly-β-cyclodextrin and a cyanine dye as a nanoplatform for two-photon imaging of ascorbic acid in living cells and tissue, Microchim. Acta 186 (2019) 201.
[26] J.B. Ghasemi, M.K. Rofouei, N. Amiri, Using chemometric methods for overlap correction of sodium–zinc spectral lines generated by wavelength dispersive X-ray fluorescence in mineral samples, X-Ray Spectrom. 43 (2014) 131–137.
[27] F. Hasanpour, A.A. Ensafi, T. Khayamian, Simultaneous chemiluminescence determination of amoxicillin and clavulanic acid using least squares support vector regression, Anal. Chim. Acta 670 (2010) 44–50.
[28] G. Wang, Y.-A. Sun, Q. Ding, C. Dong, D. Fu, C. Li, Estimation of source spectra profiles and simultaneous determination of polycomponent in mixtures from ultraviolet spectra data using kernel independent component analysis and support vector regression, Anal. Chim. Acta 594 (2007) 101–106.
[29] A.A. Ensafi, M. Taei, T. Khayamian, F. Hasanpour, Simultaneous voltammetric determination of enrofloxacin and ciprofloxacin in urine and plasma using multiwall carbon nanotubes modified glassy carbon electrode by least-squares support vector machines, Anal Sciences 26 (2010) 803–808.
[30] Y. Xia, S. Gan, Q. Xu, X. Qiu, P. Gao, S. Huang, A three-way junction aptasensor for lysozyme detection, Biosens. Bioelectron. 39 (2013) 250–254.
[31] Z. Guo, Z. Zhu, X. Zhang, Y. Chen, Facile synthesis of blue-emitting carbon dots@mesoporous silica composite spheres, Solid State Sci. 76 (2018) 100–104.
[32] A.A. Ensafi, P. Nasr-Esfahani, B. Rezaei, Synthesis of molecularly imprinted polymer on carbon quantum dots as an optical sensor for selective fluorescent determination of promethazine hydrochloride, Sensors and Actuators B: Chem. 257 (2018) 889–896.
[33] F. Sun, Z. Wang, Y. Feng, Y. Cheng, H. Ju, Y. Quan, Electrochemiluminescent resonance energy transfer of polymer dots for aptasensing, Biosens. Bioelectron. 100 (2018) 28–34.
[34] Z. Saberi, B. Rezaei, H. Faroukhpour, A.A. Ensafi, A fluorometric aptasensor for methamphetamine based on fluorescence resonance energy transfer using cobalt oxyhydroxide nanosheets and carbon dots, Microchim. Acta 185 (2018) 303.
[35] Q. Nie, Q. Cai, H. Xu, Z. Qiao, Z. Li, A facile colorimetric method for highly sensitive ascorbic acid detection by using CoOOH nanosheets, Anal. Methods 10 (2018) 2623–2628.
[36] A. Niazi, J.B. Ghasemi, A. Yazdanipour, Simultaneous spectrophotometric determination of nitroaniline isomers after cloud point extraction by using least-squares support vector machines, Spectrochim Acta Part A 68 (2007) 523–530.